PHYSICS

Realization of thousand-second improved confinement plasma with Super I-mode in Tokamak EAST

Yuntao Song[1]*, Xiaolan Zou[2]*, Xianzu Gong[1]*, Alain Becoulet[2]†, Richard Buttery[3], Paul Bonoli[4], Tuong Hoang[1], Rajesh Maingi[5], Jinping Qian[1], Xiaoming Zhong[6], Adi Liu[6], Erzhong Li[1], Rui Ding[1], Juan Huang[1], Qing Zang[1], Haiqing Liu[1], Liang Wang[1], Ling Zhang[1], Guoqiang Li[1], Youwen Sun[1], Andrea Garofalo[3], Tom Osborne[3], Tony Leonard[3], Seung Gyou Baek[4], Greg Wallace[4], Liqing Xu[1], Bin Zhang[1], Shouxin Wang[1], Yuqi Chu[1], Tao Zhang[1], Yanmin Duan[1], Hui Lian[1], Xuexi Zhang[1], Yifei Jin[1], Long Zeng[1], Bo Lyu[1], Binjia Xiao[1], Yao Huang[1], Yong Wang[1], Biao Shen[1], Nong Xiang[1], Yu Wu[1], Jiefeng Wu[1], Xiaojie Wang[1], Bojiang Ding[1], Miaohui Li[1], Xinjun Zhang[1], Chengming Qin[1], Weibin Xi[1], Jian Zhang[1], Liansheng Huang[1], Damao Yao[1], Yanlan Hu[1], Guizhong Zuo[1], Qiping Yuan[1], Zhiwei Zhou[1], Mao Wang[1], Handong Xu[1], Yahong Xie[1], Zhengchu Wang[1], Junling Chen[1], Guosheng Xu[1], Jiansheng Hu[1], Kun Lu[1], Fukun Liu[1], Xinchao Wu[1], Baonian Wan[1], Jiangang Li[1], EAST Team

Mastering nuclear fusion, which is an abundant, safe, and environmentally competitive energy, is a great challenge for humanity. Tokamak represents one of the most promising paths toward controlled fusion. Obtaining a high-performance, steady-state, and long-pulse plasma regime remains a critical issue. Recently, a big breakthrough in steady-state operation was made on the Experimental Advanced Superconducting Tokamak (EAST). A steady-state plasma with a world-record pulse length of 1056 s was obtained, where the density and the divertor peak heat flux were well controlled, with no core impurity accumulation, and a new high-confinement and self-organizing regime (Super I-mode = I-mode + e-ITB) was discovered and demonstrated. These achievements contribute to the integration of fusion plasma technology and physics, which is essential to operate next-step devices.

INTRODUCTION

With increasing global energy demand, our current energy sources, mainly fossil fuel reserves, must be substantially substituted with alternative nonfossil ones. Potential candidates include renewable and nuclear fission and fusion sources. Nuclear fusion, which powers the Sun, is the least developed of the three but is advantageous in terms of safety (only small quantities of nuclear waste with a short life generated) and environmental friendliness (no carbon dioxide generation), offering a virtually inexhaustible energy source. Fusion research has concentrated primarily on high peak performance, with considerable progress having been made toward the generation of fusion energy, namely, in Tokamak Fusion Test Reactor (TFTR) (*1*) and Joint European Torus (JET) (*2*). However, to ensure the feasibility of fusion reactors, the plasma performance must be sustained for long durations, which is often limited by the capacity of the machine and its subsystems and the plasma scenario development depending on the physics. Continuous operation of fusion reactors requires superconducting magnets, heating systems with a long-pulse capability, cooled plasma-facing components (PFCs) with the ability to handle injected power and ultimately the fusion power, and diagnostics and real-time feedback control algorithms for controlling the plasma. Steady-state and long-pulse operation with improved energy confinement with new plasma physics progress would be highly desirable for the fusion reactor, for both technological and economic reasons. There are two key physics issues for the fusion reactor: (i) to find a candidate high-confinement scenario without edge instability, like edge-localized modes (ELMs), and compatible with high-performance core plasma with internal transport barrier (ITB) and (ii) to demonstrate the plasma scenario stationarity of long duration, for example, hundreds seconds for the plasma density control (particle exhaust and recycling, wall saturation), and up to thousands seconds for material erosion. It should be noted that the multiple interactions between technology and physics can only be completed evaluated in long-duration discharges. Equally important are various weak physics phenomena that do not appear on short time scales but whose cumulative effect can become a serious problem when integrated over a long period, typically up to thousands seconds as mentioned.

Nearly all current magnetic confinement fusion devices rely on superconducting coil technology for steady-state and long-pulse operation, including Experimental Advanced Superconducting Tokamak (EAST) (*3*), Japan Tokamak 60 Super Advanced (JT60-SA) (Japan), Korea Superconducting Tokamak Advanced Research (KSTAR) (Korea), Superconducting Steady State Tokamak 1 (SST1) (India), W Environment in Steady-State Tokamak (WEST) (France), Wendelstein 7-X (W7X) (Germany), as well as the

[1]Institute of Plasma Physics, Chinese Academy of Sciences, Hefei 230031, China. [2]CEA, IRFM, F-13108 St Paul Les Durance, France. [3]General Atomics, PO Box 85608, San Diego, CA 92186-5608, USA. [4]Plasma Science and Fusion Center, Massachusetts Institute of Technology, Cambridge, MA, 02139, USA. [5]Princeton Plasma Physics Laboratory, Princeton, NJ 08543, USA. [6]University of Science and Technology of China, Hefei, Anhui 230026, China.
*Corresponding author. Email: songyt@ipp.ac.cn (Y.So.); xiao-lan.zou@cea.fr (X.Zo.); xz_gong@ipp.ac.cn (X.G.)
†Present address: ITER Organization, Route de Vinon sur Verdon, 13115 St Paul Lez Durance, France.

major next-step tokamaks: International Thermonuclear Experimental Reactor (ITER) (*4*) and China Fusion Engineering Test Reactor (CFETR) (*5*). For above magnetic confinement fusion devices, from the point of view of the characteristic time scale related to physics events and technological constraints in a long-pulse operation, we gradually encounter a time scale ranging from milliseconds for magnetohydrodynamic (MHD) events, to seconds for the energy and particle confinement time, to tens seconds for the current diffusion time, and the PFC cooling, to hundreds seconds for the plasma-wall interaction (PWI), such as wall saturation, and up to thousands seconds for material erosion (*6*). The role of actively cooled PFCs is to protect the in-vessel materials against plasma particles and thermal loads (*7*, *8*). The PFC cooling time scale denotes the time to reach a stationary temperature for PFCs (*9*). EAST is one of large tokamaks operating long-pulse discharges, which has included actively cooled PFCs, with a continuous scheme of development to improve their performances and their reliability (*10*). Wall saturation is mainly resulting from H/D retention by the wall, which has strong impact on the density control (*11*). The erosion of PFCs under plasma exposure during long-pulse operation can affect their thermal and mechanical properties, thus limiting their lifetime [(*12*) and references therein]. The erosion mechanisms for materials such as tungsten are physical and chemical sputtering and evaporation, including the eventual partial loss of the melt layer (*13*, *14*). The thermal wall loads, expected for ITER in the deuterium-tritium phase, are envisaged to be as high as 20 MW m^{-2} on the divertor plates, and the typical pulse length of plasma discharges will be >450 s (*15*). For a fusion reactor, 1000 s can be considered as a reasonable time scale for viability demonstration. The main scientific mission goals of the ITER is to demonstrate controlled ignition and extended burn for a duration sufficient to achieve stationary conditions on all time scales characteristic of plasma process and PWIs (heat and particle handling, impurity generation, fuel retention, PFC material erosion, etc.) and sufficient for achieving stationary conditions for nuclear testing of blanket components. This can be fulfilled by pulses with plasma burn duration in the range of 1000 s (*16*). One of planned basic operation scenarios for ITER is "hybrid scenario": long-pulse, inductive, and noninductive deuterium-tritium plasma scenario with current profile control, improved H-mode confinement aiming at maintaining substantial fusion power (>300 MW, fusion energy gain factor $Q = 5$) at a medium safety factor ($q_{95} = 4$) for burn duration of up to 1000 s. This plasma scenario would allow the characterization of key aspects of PWI in the ITER environment over very long durations (e.g., impact on fueling, erosion/redeposition, and fuel retention) (*17*). It should be noted that for DEMO, the next-step fusion reactor after ITER, it must resolve all physics and technical issues foreseen in the plant and demonstrate reactor relevant technologies, demonstrate the production of several 100 MW of electricity, demonstrate the breeding capability with the blanket modules that would lead to tritium self-sufficiency for fusion fuel, and achieve adequate availability/reliability over a time period of 2 hours (7200 s) (*18*).

It is crucial to develop a novel candidate scenario, which has high-energy confinement without ELMs and can be sustained over 1000 s in steady state. This is the mission of the "steady-state and long-pulse operation" path, which is one of two complementary approaches for magnetic fusion research. The other one is the "performance" path, where controlled fusion is carried out for a few seconds with mega-ampere and megawatt class tokamaks, such as JET and TFTR.

EAST is a medium-sized fully superconducting tokamak with actively cooled metallic PFCs, applying the same concept as ITER and CFETR. It has ITER-like magnetic configurations: major radius $R = 1.85$ m, minor radius $a = 0.45$ m, plasma current $I_p = 1$ MA, and toroidal field $B_T = 3.5$ T. Its mission is to address key technological and physics issues of long-pulse operation to support the design of reactor-grade machines. It is equipped with a total heating and current drive power of 32 MW, including neutral beam injection (NBI) heating of 8 MW and radio frequency (RF) power of 24 MW: (i) lower hybrid current drive (LHCD) of 10 MW (4 MW at 2.45 GHz and 6 MW at 4.6GHz); (ii) electron cyclotron resonance frequency heating (ECRH) of 2 MW at 140 GHz; and (iii) ion cyclotron resonance frequency heating (ICRH) of 12 MW at 27 to 80 MHz. With the moderate total injected power, EAST can demonstrate a significant total injected energy with steady-state thousand-second operation for ITER and future fusion devices on the way of the steady-state and long-pulse operation. The total injected energy represents the machine's ability to support and extract heat. For example, 1 GJ of injected energy obtained on Tore Supra in 2004 during a discharge constituted a world record for a tokamak at that time. In this approach for fusion research, elevated capabilities of EAST were achieved in recent experiment. EAST's ITER-like tungsten (W) divertor has a steady-state power handling capability of ~10 MW m^{-2} for addressing PWI physics. In addition, approximately 80 advanced diagnostics have been developed and implemented on EAST. These diagnostics allow the dynamics of plasma profiles, instabilities, and PWIs to be measured during long-pulse operations. Therefore, EAST is a suitable platform to integrate technology and physics related to the long-duration operation of fusion plasmas (*3*). In particular, EAST, especially its divertor, can provide an ideal plasma-wall equilibrium to study the physics of PWIs for next-step devices.

As mentioned, ITER (*19*) and CFETR are designed for steady-state operation with a duration of over 1000 s. Previously, discharges lasting over 6 min have been achieved in Tore Supra (*20*), HT-7 (*21*), and EAST (*22*). In 2021, EAST reached a milestone, achieving steady-state plasma with improved energy confinement that could be operated for a duration exceeding 1000 s and with injected/extracted energy of 2 GJ. This demonstrates the reliability of the machine and its subsystems (cryogenic, superconducting magnets, heating systems, and diagnostics) for steady-state long-pulse operation and advanced scenario. Heat and particle fluxes in the divertor target plates were actively controlled during the discharge for over 1056 s. A physical phenomenon related to the improved energy confinement was discovered. The plasma regime, which we term "Super I-mode," is characterized by the coexistence of an electron ITB (e-ITB) at the plasma center and an improvement energy confinement mode (I-mode), without ELMs, at the plasma edge, leading to a large improved energy confinement. Discharges lasting from a few ten seconds to a thousand seconds showed an energy confinement much higher than that of the low-confinement plasma (L-mode), and comparable to the high-confinement mode (H-mode), heat fluxes on PFCs and the divertor remained at moderate values, and steady-state peak heat flux on the divertor target plates was well controlled, which is envisaged as the basic operating mode of ITER.

RESULTS

To access long-duration plasmas, experiments have been performed in a double-null magnetic configuration mainly using LHCD and ECRH at I_p = 300 to 400 kA, B_T = 2.75 T, R = 1.91 m, and a = 0.45 m. B_T was chosen to be 2.75 T to simultaneously achieve on-axis ECRH deposition and optimized LHCD power absorption at 4.6 GHz. The line-averaged electron density $\overline{n}_e$ was approximately 2×10^{19} m^{-3}. The operational conditions were carefully tuned shot by shot, keeping the main parameters, such as heating powers, plasma density, plasma current, and plasma shape, the same.

Both particles and heat exhaust related to PWI must be controlled to operate long pulses. Therefore, real-time feedback control was implemented on EAST using additional relevant techniques. The plasma configuration is double null (DN) during discharge to avoid excessive heat flux on PFCs. A powder dropper was used to inject lithium to mitigate impurities and reduce recycling. This allows control of density and radiated power due to impurities. Note that low particle recycling is favorable for cryo-pumping, which does not suffer from saturation or release of particles back into the plasma when in a low recycling regime.

Repeated tests of the plasma control system (PCS) were performed each day before the experiments to minimize the error due to the offset of integrators of magnetic measurements, which is essential for controlling both the position (zero shift) and shape of the plasmas. Thus, a stable gap (~4 cm) between the plasma and the wall was maintained in the DN configuration, ensuring sufficient particle exhaust.

After repetitive discharges of hundreds of seconds, a discharge with a duration of 1056 s was achieved, as shown in Fig. 1. A total energy of 2 GJ was injected into the plasma, twice as much as the record previously held by Tore Supra and EAST. The plasma was operated at I_p = 330 kA and $\overline{n}_e = 1.8 \times 10^{19}$ m^{-3}; it was heated by a total RF power of 1.65 MW (1.1 MW of LHCD at 4.6 GHz and 0.55 MW of ECRH). As shown in the figure, all the main plasma quantities are stationary during the entire discharge. The radiation power, with tungsten as the major radiating species, is found to be very low (~150 kW). Note that the discharge is fully noninductive, i.e., the plasma current is mainly driven by LHCD and a moderate bootstrap current (~37%). As illustrated in Fig. 2, in the 1056-s discharge, which is called the Super I-mode, will be described in detail below, the corresponding LHCD efficiency estimated by $\eta_{CD} = \frac{I_{LH} n_e R}{P_{LH}}$ (A/W/m^2) (*23*) is ~0.87×10^{19} A W^{-1} m^{-2}. The current drive efficiency in this discharge is comparable to the experimental value in L-mode plasma, but slightly lower than that in H-mode plasma, where I_{LH} and P_{LH} are the lower hybrid driven current and lower hybrid wave power, respectively.

Plasma-wall interactions

PWI is not an operational issue in the long-pulse experiments discussed in this study. During 1000 s, the particle flux on the divertor remained extremely stable, and the global recycling coefficient R_{global} was stationary at ~0.95, as shown in Fig. 3C. This is due to the optimization of the strike point position to realize better particle exhaust, along with enhanced wall pumping using real-time wall conditioning by continuous lithium powder injection (1.3 mg/s) from t = 7 s until the end of the discharge, which can effectively getter deuterium. Particle balance is used to evaluate the wall pumping capability, and the results show that, during the 1056 s discharge, the pumping rate of the divertor cryopumps is (7.3 to 8.1) × 10^{19} D-atoms/s, and that of the first wall is (7.9 to 12.9) × 10^{19} D-atoms/s. This indicates that the first wall assisted by lithium injection has even stronger pumping capability than the divertor cryopumps, the wall pumping rate is ~1.4 times higher than that of the divertor cryopumps, and the wall is not saturated even at the end of the discharge, as shown in Fig. 3. Thus, EAST is a platform for studying the physics of PWIs under ideal conditions where plasma,-wall equilibrium—on the time scale of tens of minutes—is required.

Heat fluxes on PFCs and the divertor remained at moderate values. Steady-state peak heat flux on the divertor target plates was well controlled, remaining below 3 MW/m^2 (Fig. 1D), considerably lower than the power exhaust capability of the water-cooled tungsten divertor in EAST (10 MW/m^2).

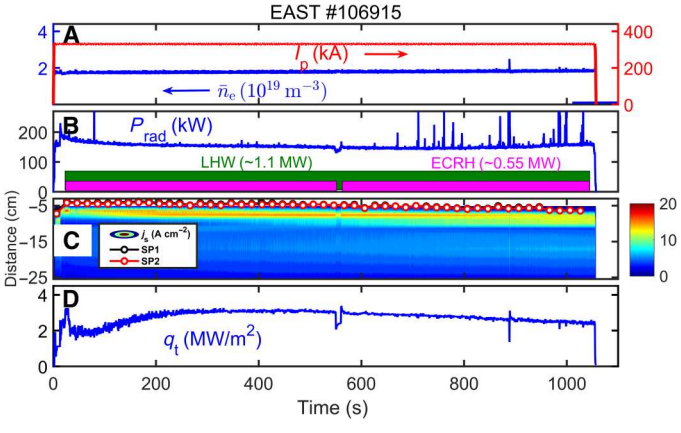

Fig. 1. Waveform of the thousand-second discharge #106915. (**A**) Plasma current I_p and line-averaged electron density $\overline{n}_e$. (**B**) LHCD, ECRH, and radiated powers. (**C**) Contour of particle flux given by the ion saturation current j_s on the divertor target, with the strike points calculated from EFIT equilibrium shown in open circles (SP1 and SP2 are outer strike points for two *X*-points in double-null configuration, respectively). (**D**) Peak heat flux on the divertor target.

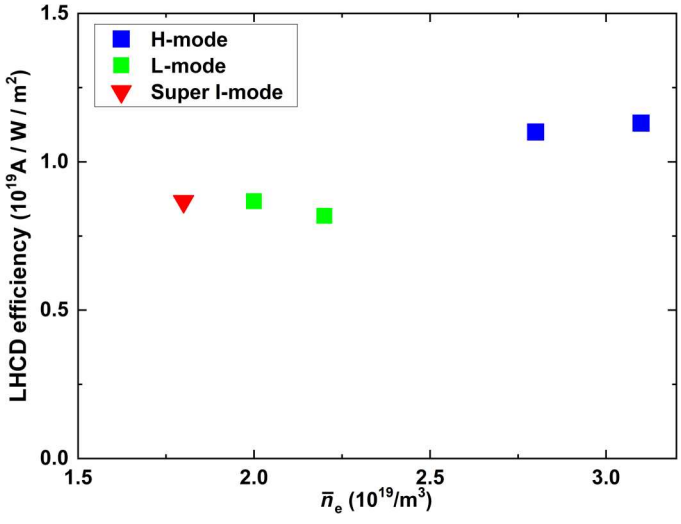

Fig. 2. LHCD efficiency. Experimental comparison of LHCD efficiency in the L-mode, H-mode, and Super I-mode.

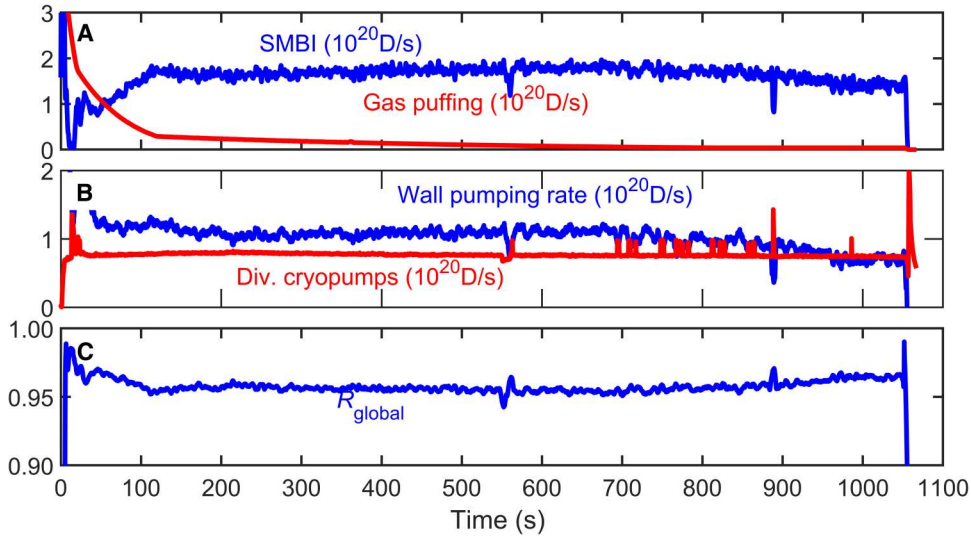

Fig. 3. Pumping rate and global recycling. (**A**) Gas injection rate of supersonic molecular beam injection (SMBI) and gas puffing. (**B**) Pumping rate of divertor cryopumps and the first wall. (**C**) Global recycling coefficient.

Extreme ultraviolet (EUV) spectroscopic measurements indicate the low concentrations of light and heavy impurities, which is consistent with the low radiated power shown in Fig. 1B. W impurity is the dominant factor contributing to total radiation power loss. The concentration of W is considerably lower than that of a similar discharge observed in H-mode, as shown in Fig. 4. Such a low W concentration can be explained by the L-mode–like particle transport, an insufficient W source observed in the absence of ELMs, and because of the optimization of plasma current, RF heating power coupling, and real-time Li powder injection. Moreover, the divertor electron temperature measured by Langmuir probes is 15 to 20 eV during the discharge, favoring a relatively low W source, which exhibits a strong dependence on electron temperature at the target plates.

Note that W was not accumulated in the core plasma over 1000 s. This behavior is similar to that observed in WEST plasmas heated by RF powers, which is attributed to the low torque driven by the RF waves (*24*). Note that the increase in central W accumulation is due to the neoclassical convection increasing with toroidal rotation. Therefore, the result obtained is promising for low torque operation in ITER.

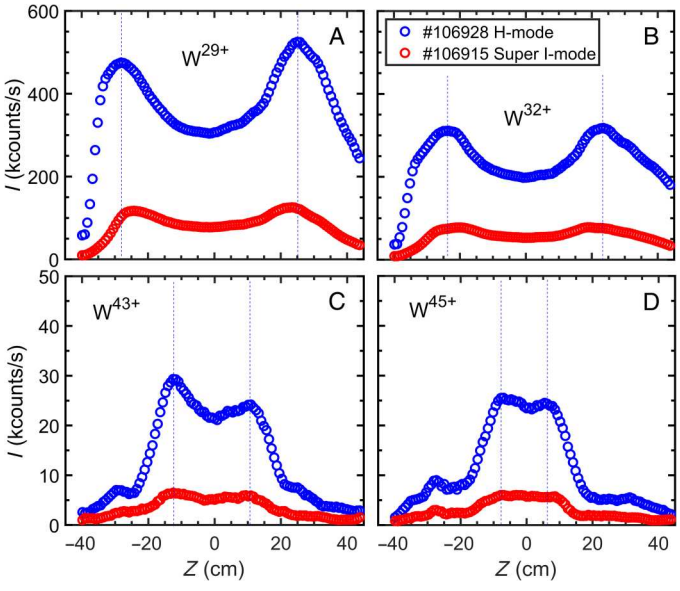

Fig. 4. Tungsten (W) impurity radiation. Line intensity profiles of W ions in discharge #106915, compared with discharge operated in H-mode (#106928: I_p = 400 kA, 2 MW of LHCD, 1 MW of ECRH). (**A**) W^{29+}, (**B**) W^{32+}, (**C**) W^{43+}, and (**D**) W^{45+} ions observed by space-resolved EUV spectrometers (vertical dashed lines indicate peak position of line intensities in H-mode).

Super I-mode

H-mode (*25*), characterized by the edge transport barriers (ETBs) of both density and temperature profiles, is considered as the baseline operation scenario for ITER. Unacceptable heat flux to the divertor targets caused by large ELMs due to the relaxation of the ETB is still a crucial issue in fusion research (*26*). For a fusion reactor, the ideal situation would be to have high-energy confinement and reasonable particle confinement. I-mode meets this criterion better than H-mode. I-mode is a plasma regime with energy confinement similar to that in H-mode, and edge particle transport comparable to that in L-mode. I-mode was initially discovered on Alcator C-Mod (*27*) and ASDEX Upgrade (*28*) and is characterized by an extremely steep edge temperature pedestal with the absence of the edge density pedestal and ELMs. The I-mode operation regime has several advantages over H-mode, such as preventing metallic impurity central accumulation, facilitating fusion product ash removal, and sustaining quiet stationary temperature pedestal and thus is more suitable for application in the fusion reactor. A regime with double transport barrier combining ITB and I-mode, named as Super I-mode, was discovered in discharges with durations ranging from 14 to 1055 s. It could be interesting for ITER as a candidate scenario, which has high-energy confinement without ELMs and can be sustained over 1000 s in steady state.

In the EAST tokamak, stationary I-mode is also identified by the weakly coherent mode (WCM) (*29*) and edge temperature ring

oscillation (ETRO) (*30*). The ETRO, radially localized at the pedestal with an azimuthally symmetric structure, results from the ion/electron turbulence periodic transition. The WCM corresponds to electron turbulence, leading to L-mode–like particle transport. The stationarity of I-mode is due to the plasma self-organization by coupling electron temperature gradient oscillation, turbulence transition, and heat transport modulation (*29*).

The energy confinement of discharge #106915 matches that of the one predicted in H-mode. The confinement time τ_E is higher than the value predicted by the H-mode scaling law $\tau^H_{\mathrm{Scaling},98y2}$ (*31*) by 20% and the energy confinement enhancement factor $H_{98} = \tau_E/\tau^H_{\mathrm{Scaling},98y2} = 1.2$ (Fig. 5A). The plasma stored energy is 90 kJ, corresponding to the normalized plasma pressure $\beta_p = \langle p\rangle/(B_p{}^2/2\mu_0) \sim 1.5$, which is the ratio of the plasma pressure to the magnetic field pressure. Here, $\langle p\rangle$ is the mean plasma pressure and B_p is the poloidal magnetic field. The central electron temperature T_e (0) exceeds 6 keV and remains almost constant throughout the discharge (Fig. 5B). The central ion temperature T_i (0) is about 0.7 keV.

I-mode is identified in discharge #106915 by detecting both WCM and ETRO, which are obtained from the power frequency spectrum of the time derivative of the density fluctuation phase dϕ/dt, measured using a Doppler reflectometer (DR) at the normalized radius $\rho = 0.91$, and lasts for almost the whole discharge, as shown in Fig. 5 (C and D). The brief anomaly observed in WCM and ETRO spectra around $t = 570$ s is due to a sudden and brief protection of the gyrotron (see Fig. 1B). The WCM frequency is in the range of 30 to 100 kHz, while the ETRO frequency is approximately 14 kHz.

High confinement is related to evident improvements in both core and edge plasma. Figure 6 (A and B) displays in red the radial profiles of the electron temperature and density of the discharge #106915, respectively. Then, these profiles are compared to those of L-mode (#106870, in blue) and H-mode (#107832, in green) plasma. An e-ITB is observed at the plasma center in the discharge #106915 as the H-mode, leading to a peaked central electron temperature. Simultaneously, an electron temperature pedestal is observed in this discharge at the plasma edge, similar to that in H-mode, as shown in Fig. 6C. However, in the absence of the pedestal, the edge density profile is extremely similar to that in L-mode, as shown in Fig. 6D.

In discharge #106915, the electron temperature profile was found to be strongly peaked in $\rho < 0.4$, exhibiting good correlation with the e-ITB location. The election thermal conductivity, obtained via a power balance analysis, decreases significantly to the neoclassical value at $\rho = 0$ to 0.4 and $\rho = 0.9$ to 1.0, as shown in Fig. 6E, confirming the presence of an ETB (I-mode) and a core ITB.

The MHD activities are continuously present in the plasma center throughout this long pulse discharge (Fig. 7B). Figure 7A displays the safety factor q profile measured using a polarimeter-interferometer (POINT) in I-mode. A flat central q profile was identified by POINT to clamp the central q at values close to unity with $q_{95} = 9.3$. Figure 7 (C to E) shows the magnified view ($t = 17.8$ to 19 s) of the MHD intensity, the normalized electron temperature gradient R/L_{Te} (L_{Te}=(∇ $T_e/T_e)^{-1}$), and the turbulence intensity, respectively. It was observed that these latter three signals are modulated at the same frequency, indicating a strong interaction between MHD, turbulence, and heat transport. The core e-ITB is identical to that observed in the long-pulse H-mode discharges as shown in Fig. 6. The physical mechanism for maintaining this e-ITB has been elucidated in (*32*) as follows. The electron-temperature-gradient–driven mode (ETG) is excited when R/L_{Te} is above a threshold

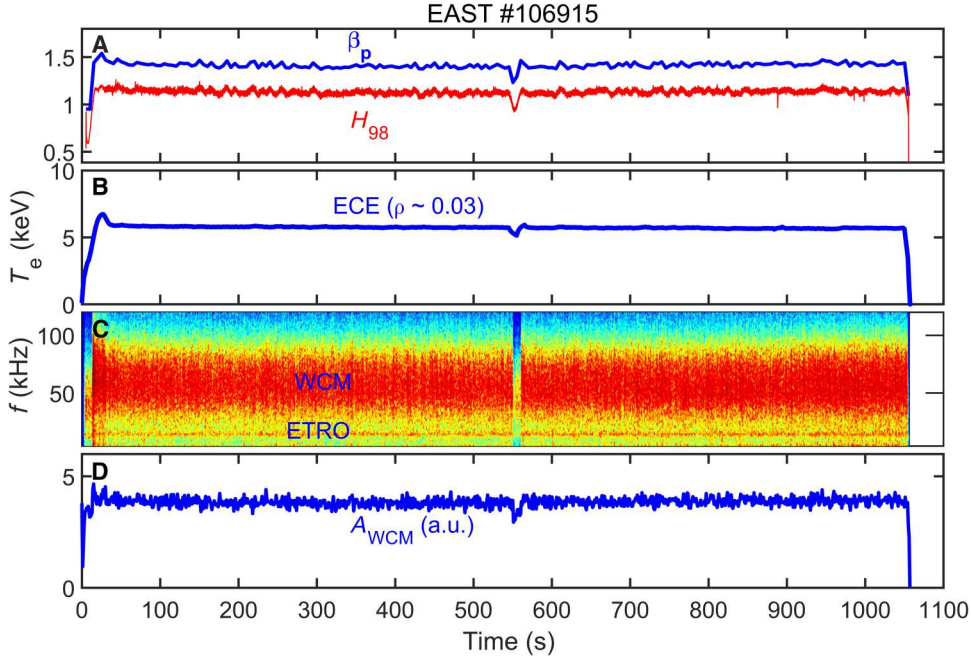

Fig. 5. I-mode identification. (**A**) Energy confinement enhancement factor H_{98} and the normalized plasma pressure β_p. (**B**) Electron temperature T_e measured at $\rho = 0.03$ by electron cyclotron emission (ECE) diagnostic. Note that the central ECE measurement is less affected by the suprathermal electrons generated by LHCD and is also calibrated with Thomson scattering. (**C**) Frequency spectrogram of the time derivative of the density fluctuation phase dϕ/dt measured using a Doppler reflectometer at $\rho = 0.91$, showing WCM (30 to 100 kHz) and ETRO (14 kHz). (**D**) Amplitude of WCM. a.u., arbitrary units.

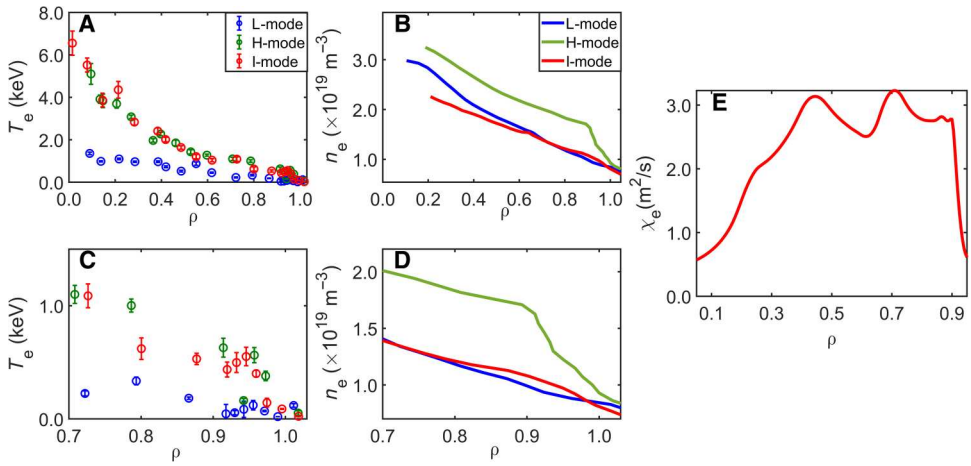

Fig. 6. Electron temperature and density profiles for transport analysis. The temperature and density radial profiles of Super I-mode (discharge #106915, in red) are compared to those of the H-mode (discharge #107832, in green) and L-mode (discharge #106870, in blue). (**A**) Electron temperature profiles from the Thomson scattering diagnostic, showing evident ITB for Super I-mode and H-mode. (**B**) Electron density profile from the reflectometer. (**C**) Zoomed view of the electron temperature profile at the edge for better differentiating the pedestal of Super I-mode from L-mode. (**D**) Zoomed view of the electron density profile at the edge, showing similar edge density profile for Super I-mode and L-mode. (**E**) Electron thermal conductivity in discharge #106915, deduced from the power balance analysis.

($R/L_{Te} > 9$). Then, an intrinsic current is generated in the counter-current direction by ETG turbulence due to the divergence of the residual flux of the current, flattening the q profile at the center and weakening the central magnetic shear, which causes turbulence reduction at the plasma center. Last, the MHD mode is periodically destabilized by the high electron temperature gradient in a low magnetic shear regime, serving as a sink to release the turbulence-free energy, which causes a modulation of turbulence and turbulence-driven current. This self-regulation system serves as the automatic controller, which dynamically forces the electron temperature gradient in a proper region to sustain the kinetic equilibrium. Thus, a small amplitude oscillatory electron temperature profile around the critical temperature gradient triggering ETG is achieved, forming a quasi-stable and robust ITB.

Figure 8 represents the energy confinement enhancement factor H_{98} as a function of the pulse length for Super I-mode (solid red square), standard I-mode (red square), H-mode (blue triangle), L-mode with ITB (violet circle), and standard L-mode without ITB (black diamond) in EAST. Super I-mode has an energy confinement similar to that of H-mode but with a pulse length considerably longer than that of H-mode. Further, compared with standard I-mode, Super I-mode exhibits better energy confinement with a 50% higher H-factor. Note that the present Super I-mode was realized with a very high electron temperature and relatively lower ion temperature. Super I-mode experiments on EAST will be extended toward the case of high ion temperature.

DISCUSSION

A major advancement toward fusion reactors was recently achieved at the Institute of Plasma Physics, Chinese Academy of Sciences. A steady-state plasma was successfully maintained for over 1056 s in the fully superconducting tokamak EAST. The machine and its subsystems (cryogenic, magnets, heating systems, diagnostic, etc.) were extremely reliable and operated safely owing to the integration of real-time controls and careful prior preparation. Technology and fusion plasma physics are integrated. This achievement is mandatory to operate next-step devices, such as ITERs and CFETRs.

In addition to the operational aspect, a self-organizing, highly steady with quiet pedestal, robust plasma regime was discovered, called Super I-mode. In this regime, I-mode coexists with an e-ITB, leading to an enhancement of energy confinement with $H_{98} \sim 1.2$. Such a regime has advantages with respect to the integration of the PWI and high plasma performance on thousand-second scales. The heat load on PFCs is moderate due to the absence of ELMs; further, ITB is maintained owing to plasma self-organization without external control techniques for plasma stability. It shows that the ELMs avoidance is well compatible with high-performance core plasma in long-pulse steady-state plasma. To date, there are few experimental results in steady-state and long-pulse operation on the scale of 1000 s in the existing database. EAST is the only mega-ampere and megawatt class tokamak in the world that can reach to 1000s steady-state and long-pulse plasmas with ITER-like tungsten divertor. It is an excellent platform for research in heat load, power balance (*9*), and PWI (*33*).

As well known, currently, there are two complementary approaches for magnetic fusion research: (i) the performance path, where controlled fusion is carried out for a few seconds, which is the mission of JET (*34*), JT-60 (*35*), and TFTR (*36*); (ii) the steady-state and long-pulse operation path, which is the mission of EAST. To better illustrate the current status of tokamaks on the path to ITER, a diagram is plotted in Fig. 9, showing the fusion triple-product $[n_i(0)T_i(0)\tau_E]$ versus the plasma duration t(s) for mega-ampere and megawatt class tokamaks (JET, JT-60, Tore Supra, and EAST). Data of JT-60, JET, and Tore Supra are taken from table 3.1 in (*37*). Here, $n_i(0)$, $T_i(0)$, and τ_E are the central density, the central ion temperature, and the energy confinement time, respectively. For EAST 1000s Super I-mode plasma, $n_i(0)T_i(0)\tau_E \approx 1.3 \times 10^{18}$ m^{-3} keV s, which is represented by the large red solid circle in Fig. 9. Note that this value is quite modest compared to Lawson's criterion for ignition: $n_i(0)T_i(0)\tau_E > 3 \times 10^{21}$ (m^{-3} keV s) (*38*). In addition, the 1000s Super I-mode is a pure

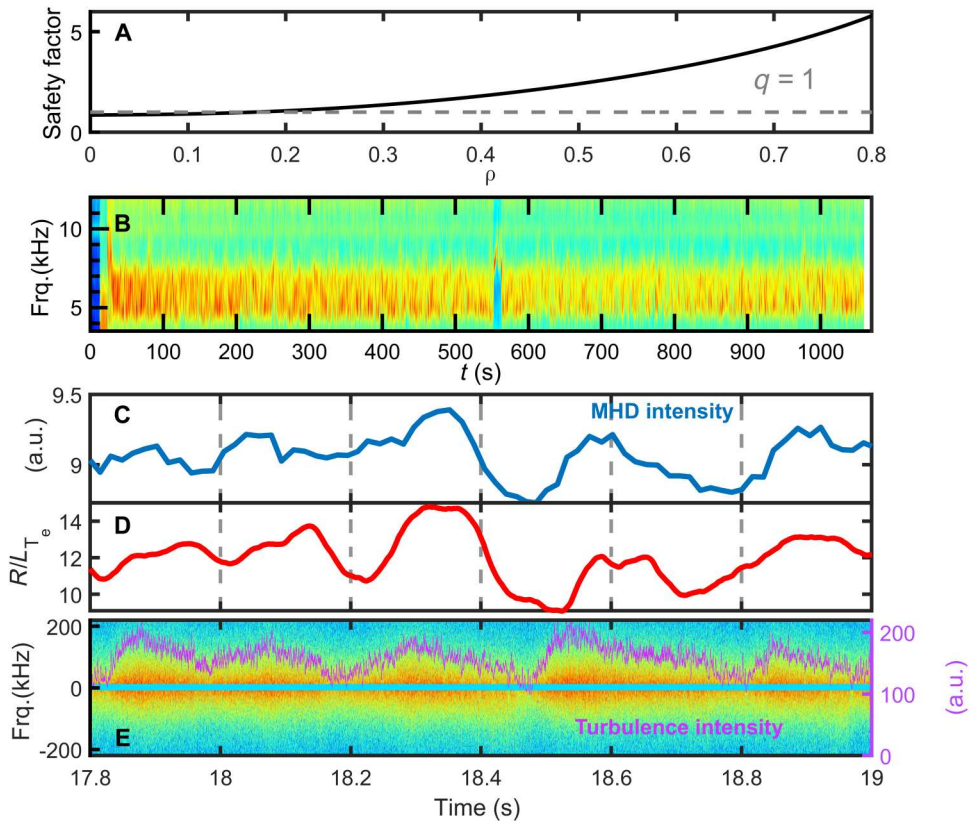

Fig. 7. Interaction between MHD, turbulence, and electron heat transport for sustaining stationary ITB. (**A**) Safety factor q reconstructed using a polarimeter-interferometer (POINT) system; q_{95} is 9.3. (**B**) MHD frequency spectrum measured in the plasma core using SXR diagnostic; the MHD frequency is in the range of 4 to 8 kHz. (**C**) Magnified view of MHD intensity at t = 17.8 to 19 s. (**D**) Normalized electron temperature gradient R/L_{Te} at t = 17.8 to 19 s. (**E**) Turbulence frequency spectrogram and intensity at t = 17.8 to 19 s.

deuterium plasma, so there was no DT fusion reaction in this experiment. EAST is planning to perform long-pulse operation experiments in the near future to increase the fusion triple product, trying to approach the ITER target. Recently, JET succeeded in injecting a power of ~30 MW (NBI + ICRF) for 5 s (total injected energy of 0.15 GJ) in a deuterium-tritium experiment. A record fusion energy of 0.059 GJ was obtained, which corresponds to an average fusion power of about 11 MW over 5 s, and a fusion energy gain factor $Q \approx 0.37$ (*39*). The main goal is to study the physics of burning plasma and that relative to energetic alpha particles produced by the fusion reaction, while the main mission of EAST is the study of physics and technology relative to stationarity and long duration. The 1000-s plasma with Super I-mode (2 GJ of injected energy) produced in EAST represents a major advance in this direction. In the future, EAST will continue to work in long-pulse discharges with more injected power. For a fusion reactor like ITER (*17*), it should combine "high performance" ($Q > 5$) and "steady state and long pulse" (burn duration > 1000 s). Even if the EAST parameters are not enough to reach the ignition and realize the deuterium-tritium fusion, the thousand-second Super I-mode regime could be interesting for ITER and fusion devices as an operational scenario. Furthermore, it is so helpful for deeply understanding the complex couplings, sometimes nonlinear, between the different physics phenomena and the multiple interactions between technology and physics in long-pulse steady-state plasma. Therefore, thousand-second Super I-mode on EAST exhibits great potential for application in ITERs and CFETRs.

MATERIALS AND METHODS

In the steady-state and long-pulse operation path, elevated capabilities of EAST were achieved in recent experiments. It is equipped with a total heating and current drive power of 32 MW, including NBI, LHCD, ECRH, and ICRH. The machine can be operated in lower single null (LSN), DN, and upper single null (USN) divertor configurations with a flexible poloidal field control system and can also periodically switch between LSN, DN, and USN configurations to facilitate long-pulse plasma operation (*40*). For controlling the highly shaped plasmas and even their dynamic, at present, the EAST team adapts the PCS, which is configured with seven real-time processes running on seven corresponding physical central processing unit (CPU) cores (*41*). There are two sets of RFM (reflected memory) network for diagnostic data input and control command output. All the actuator systems, such as gas puffing, power supply, and heating system, are controlled by PCS in such digital communication way, which ensures the high-quality signal transmission and plasma control performance. In the thousand-second Super I-mode experiment, PCS ensures the real-time control of the loop voltage near zero, which makes the long-pulse discharge come true (*42*). To handle the high heat fluxes during

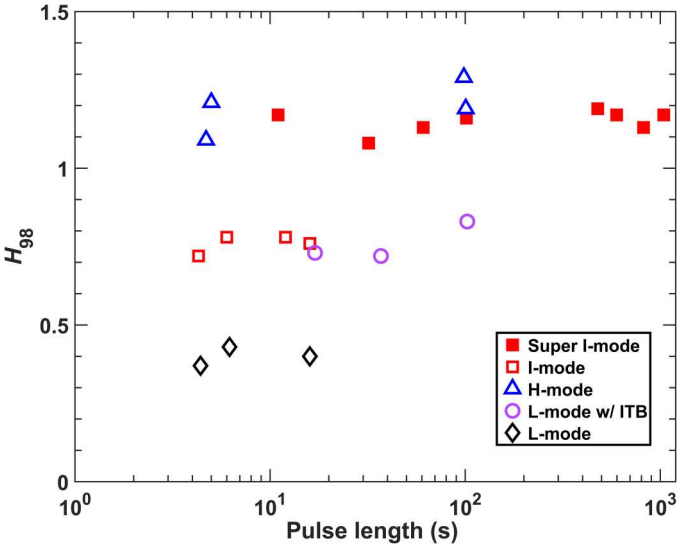

Fig. 8. Comparison of the energy confinement enhancement factor H_{98} and the plasma duration. Various plasma regimes obtained in EAST are compared: Super I-mode (solid red square), standard I-mode (red square), H-mode (blue triangle), L-mode with ITB (violet circle), and L-mode without ITB (black diamond).

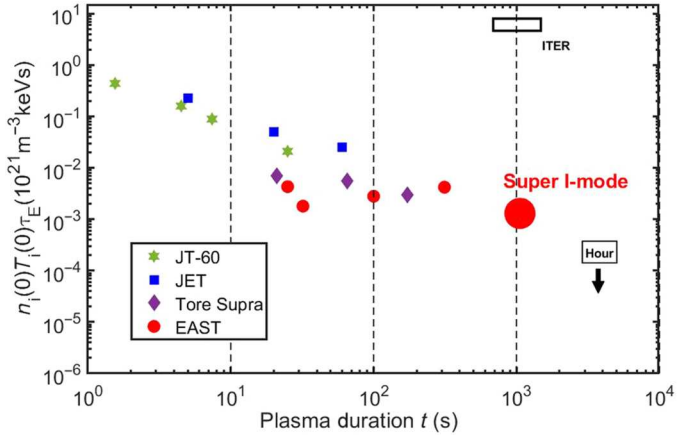

Fig. 9. Diagram of fusion triple-product $[n_i(0)T_i(0)\tau_E]$ versus plasma duration t(s) for mega-ampere and megawatt class tokamaks. Data of JT-60, JET, and Tore Supra are taken from table 3.1 in (*37*).

high-performance, steady-state discharge, all of the EAST PFCs are actively cooled. Over the past few years, EAST has been upgraded with an ITER-like active water-cooling tungsten divertor and is capable of handling a power load up to 10 MW/m^2 for long-pulse steady-state operation with high power injection and addressing PWI physics. In addition, approximately 80 advanced diagnostics have been developed and implemented on EAST. These diagnostics allow the dynamics of plasma profiles, instabilities, and PWIs to be measured during long-pulse operations. Therefore, EAST is a suitable platform to integrate technology and physics related to the thousand-second I-mode operation plasmas.

Key diagnostics for thousand-second Super I-mode physics research

On the EAST tokamak, radial profiles of key parameters and physics quantities like instabilities and turbulence of plasma could be measured. Thomson scattering system is used to measure the electron density and temperature with time resolution of 20 ms (*43*). POINT system is used for measuring plasma density and current (*44*) with spatial resolution of 8.5 cm and time resolution of 1 μs. The plasma current profile and q profile are obtained by using the Faraday rotation angle measured by POINT as additional constraint in EFIT code (*45*). EUV spectrometer system is used to measure different impurity in the thousand-second pulse and provides the space-resolved information of impurity (*46*). Using soft x-ray (SXR) system (*47*), the location of MHD is accurately determined. To understand the physics of interaction between the MHD and turbulence in this experiment, DR is applied to measure the turbulence perpendicular rotation velocity and its intensity (*48*). WCM, ETRO, and the pedestal burst instability before I-H transition are detected by the DR phase derivative perturbation in the I-mode regime (*49*). The contour of ion saturation current density j_s is obtained with the measurements of triple-Langmuir probe arrays embedded on the divertor target plates (*50*). The stationary peak heat flux is obtained from the measurements of an infrared thermography for the divertor target surface temperature. On the EAST tokamak, the reliable operation of these diagnostics ensures that we can obtain a wealth of physical information for further analysis.

Data collection system and data access

A distributed and continuous data acquisition system based on PXI/PXI Express technology has been developed for EAST. At present, the system has more than 50 data acquisition units and more than 2000 raw channels. The maximum data throughput is about 5 gigabytes/s. In case of long-term discharge mode, the raw data of one shot are more than 1 terabyte, and the total data of one campaign are more than 100 terabytes. At present, all the acquired data, except video/image, are stored into MDSplus database, which is a set of software tools for data acquisition and storage, and a methodology for management of complex scientific data (*51*). These MDSplus trees are organized as distributed mode and accessed in different servers. The distributed system can accelerate data access in general. The fast data collection system provides data access for Super I-mode plasma. Experimental data are available to any researcher with access to EAST data. The data used in this article can be read from the MDS server for EAST.

Plasma-wall interaction

Lithium coating

Lithium coating is an effective method to suppress hydrogen influx, reduce $H/(H + D)$ ratios, and reduce impurity radiation. The first lithium evaporative coating assisted by He-ICRF was performed on EAST during the 2009 campaign (*52*). Typically, Li coatings were performed every morning before plasma operation, requiring 1 to 2 hours to evaporate about 10 to 30 g. In addition, to realize real-time Li coatings, fine Li powder was injected/dropped from the upper divertor gap into plasma discharges. A flow rate of 30 to 50 mg/s was typically used using a dropper apparatus (*53*).

Pumping rate and global recycling

The pumping rate of divertor cryopumps is evaluated by the neutral pressure multiplying pumping speed in upper and lower divertor

region, and the pumping speed is calibrated before discharges. For the wall pumping rate, particle balance method is used to evaluate the pumping rate of first wall.

Global recycling coefficient (R_{global}) is evaluated by the particle balance on plasma inventory with the following equation

$$\frac{\mathrm{dNe}}{\mathrm{d}t} = (R_{\text{global}} - 1) \bullet \frac{\mathrm{Ne}}{\tau_{\mathrm{p}}} + f \bullet qQ_{\text{injection}}$$

where τ_{p} is the particle confinement time, f is the fueling efficiency of external gas injection, and $qQ_{\text{injection}}$ is the external gas injection rate (*54*).

Power balance analysis with ONETWO simulation

For the stationary state, the simplified version of the one-dimensional energy transport equation is

$$\frac{1}{V'}\frac{\partial(V'Q)}{\partial\rho} = s(\rho), \qquad Q = -\chi\partial T/\partial\rho$$

where ρ is the square root of the normalized toroidal flux, V' is the derivative of the flux surface volume with respect to ρ, Q is the energy flux, χ is the thermal conductivity (or transport coefficient), T is the temperature, and s is the integrated energy source. Electron thermal conductivity in discharge #106915 is deduced from the power balance analysis. The energy source is from ECRH and lower hybrid wave (LHW). In ONETWO code, $V'(\rho)$ is calculated by the reconstructed equilibria, $T(\rho)$ is from the experimental measurements, and $s(\rho)$ is calculated by the TORAY-GA and GENRAY codes using the equilibria and kinetic profiles from experiment.

Supplementary Materials

This PDF file includes:

Supplementary Text
Tables S1 and S2
References

REFERENCES AND NOTES

1. M. G. Bell, K. M. McGuire, V. Arunasalam, C. W. Barnes, S. H. Batha, G. Bateman, M. A. Beer, R. E. Bell, M. Bitter, N. L. Bretz, R. V. Budny, C. E. Bush, S. R. Cauffman, Z. Chang, C.-S. Chang, C. Z. Cheng, D. S. Darrow, R. O. Dendy, W. Dorland, H. H. Duong, R. D. Durst, P. C. Efthimion, D. Ernst, H. Evenson, N. J. Fisch, R. K. Fisher, R. J. Fonck, E. D. Fredrickson, G. Y. Fu, H. P. Furth, N. N. Gorelenkov, B. Grek, L. R. Grisham, G. W. Hammett, G. R. Hanson, R. J. Hawryluk, W. W. Heidbrink, H. W. Herrmann, K. W. Hill, J. C. Hosea, H. Hsuan, M. H. Hughes, R. A. Hulse, A. C. Janos, D. L. Jassby, F. C. Jobes, D. W. Johnson, L. C. Johnson, J. Kesner, H. W. Kugel, N. T. Lam, B. Leblanc, F. M. Levinton, J. Machuzak, R. Majeski, D. K. Mansfield, E. Mazzucato, M. E. Mauel, J. M. McChesney, D. C. McCune, G. McKee, D. M. Meade, S. S. Medley, D. R. Mikkelsen, S. V. Mirnov, D. Mueller, G. A. Navratil, R. Nazikian, D. K. Owens, H. K. Park, W. Park, P. B. Parks, S. F. Paul, M. P. Petrov, C. K. Phillips, M. W. Phillips, C. S. Pitcher, A. T. Ramsey, M. H. Redi, G. Rewoldt, D. R. Roberts, J. H. Rogers, E. Ruskov, S. A. Sabbagh, M. Sasao, G. Schilling, J. F. Schivell, G. L. Schmidt, S. D. Scott, I. Semenov, S. Sesnic, C. H. Skinner, B. C. Stratton, J. D. Strachan, W. Stodiek, E. J. Synakowski, H. Takahashi, W. M. Tang, G. Taylor, J. L. Terry, M. E. Thompson, W. Tighe, S. V. Goeler, R. B. White, R. M. Wieland, J. R. Wilson, K.-L. Wong, P. Woskov, G. A. Wurden, M. Yamada, K. M. Young, M. C. Zarnstorff, S. J. Zweben, Overview of DT results from TFTR. *Nucl. Fusion* **35**, 1429–1436 (1995).
2. J. Jacquinot, V. P. Bhatnagar, J. G. Cordey, L. D. Horton, D. F. H. Start, R. Barnsley, P. Breger, J. P. Christiansen, S. Clement, S. J. Davies, J. K. Ehrenberg, L.-G. Eriksson, G. M. Fishpool, M. Gadeberg, P. J. Harbour, H. J. Jäckel, K. Lawson, J. Lingertat, C. G. Lowry, C. F. Maggi, G. F. Matthews, R. D. Monk, D. P. O'Brien, E. Righi, G. Saibene, R. Sartori, B. Schunke, A. C. C. Sips, M. F. Stamp, D. Stork, J. D. Strachan, A. Tanga, K. Thomsen; JET Team, Overview of ITER physics deuterium-tritium experiments in JET. *Nucl. Fusion* **39**, 235–253 (1999).
3. J. Li, H. Y. Guo, B. N. Wan, X. Z. Gong, Y. F. Liang, G. S. Xu, K. F. Gan, J. S. Hu, H. Q. Wang, L. Wang, L. Zeng, Y. P. Zhao, P. Denner, G. L. Jackson, A. Loarte, R. Maingi, J. E. Menard, M. Rack, X. L. Zou, A long-pulse high-confinement plasma regime in the Experimental Advanced Superconducting Tokamak. *Nat. Phys.* **9**, 817–821 (2013).
4. ITER, http://www.iter.org/.
5. Y. Wan, J. Li, Y. Liu, X. Wang, V. Chan, C. Chen, X. Duan, P. Fu, X. Gao, K. Feng, S. Liu, Y. Song, P. Weng, B. Wan, F. Wan, H. Wang, S. Wu, M. Ye, Q. Yang, G. Zheng, G. Zhuang, Q. Li, Overview of the present progress and activities on the CFETR. *Nucl. Fusion* **57**, 102009 (2017).
6. A. Becoulet, G. T. Hoang, The technology and science of steady-state operation in magnetically confined plasmas. *Plasma Phys. Control. Fusion* **50**, 124055 (2008).
7. Tore Supra team presented by J.J. Cordier, Tore Supra experience on actively cooled high heat flux components. *Fusion Eng. Des.* **61–62**, 71–80 (2002).
8. Y. T. Song, X. B. Peng, H. Xie, X. F. Liu, L. M. Bao, Z. B. Zhou, L. Cao, T. J. Xu, X. Ji, Y. H. Peng, N. Zhu, P. Zhang, J. F. Wu, S. M. Wang, X. M. Wang, J. S. Hu, C. Y. Xie, J. L. Chen, G. N. Luo, D. M. Yao, D. M. Gao, X. Z. Gong, P. Fu, J. G. Li, Plasma facing components of EAST. *Fusion Eng. Des.* **85**, 2323–2327 (2010).
9. Y. K. Liu, X. Gao, K. Hanada, Y. W. Yu, H. Q. Liu, L. Yang, T. Zhang, Y. X. Jie, J. P. Qian, L. Zeng, T. F. Ming, X. J. Liu, S. C. Liu, T. J. Xu, Y. Chen, Q. Zhuang, Y. L. Li, K. F. Gan, B. Zhang, M. W. Chen, P. F. Zi, Y. M. Wang, G. S. Li, K. Z. Zhu, T. Zhou, L. Li, L. Cao, X. Z. Gong, D. M. Yao, K. Wang, L. Wang, J. G. Li; the EAST Team, Power balance investigation in long-pulse high-performance discharges with ITER-like tungsten divertor on EAST. *Nucl. Fusion* **60**, 096019 (2020).
10. J. Li, G. Luo, R. Ding, D. Yao, J. Chen, L. Cao, J. Hu, Q. Li; the EAST team, Plasma facing components for the Experimental Advanced Superconducting Tokamak and CFETR. *Phys. Scr.* **2014**, 014001 (2014).
11. N. Asakura, Wall pumping and saturation in divertor tokamaks. *Plasma Phys. Control. Fusion* **46**, B335–B347 (2004).
12. G. De Temmerman, T. Hirai, R. A. Pitts, The influence of plasma-surface interaction on the performance of tungsten at the ITER divertor vertical targets. *Plasma Phys. Control. Fusion* **60**, 044018 (2018).
13. ITER Physics Expert Group on Divertor; ITER Physics Expert Group on Divertor Modelling and Database; ITER Physics Basis Editors; ITER EDA; Naka-machi, *Nucl. Fusion* **39**, ITER Physics Basis Chapter 4: Power and particle control, 2391 (1999).
14. J. Roth, E. Tsitrone, A. Loarte, T. Loarer, G. Counsell, R. Neu, V. Philipps, S. Brezinsek, M. Lehnen, P. Coad, C. Grisolia, K. Schmid, K. Krieger, A. Kallenbach, B. Lipschultz, R. Doerner, R. Causey, V. Alimov, W. Shu, O. Ogorodnikova, A. Kirschner, G. Federici, A. Kukushkin; EFDA PWI Task Force, ITER PWI Team, Fusion for Energy, ITPA SOL/DIV, Recent analysis of key plasma wall interactions issues for ITER. *J. Nucl. Mater.* **390–391**, 1–9 (2009).
15. J. Linke, J. Du, T. Loewenhoff, G. Pintsuk, B. Spilker, I. Steudel, M. Wirtz, Challenges for plasma-facing components in nuclear fusion. *Matter Radiat. Extremes* **4**, 056201 (2019).
16. ITER Physics Basis Editors; ITER Physics Expert Group Chairs and Co-Chairs; ITER Joint Central Team and Physics Integration Unit; ITER EDA; Naka-machi, Overview and summary. *Nucl. Fusion* **39**, 2137 (1999).
17. ITER Organization, ITER research plan within the staged approach (level III – provisional version) (ITER Technical Report No. ITR-18-003, 2018).
18. G. Federici, R. Kemp, D. Ward, C. Bachmann, T. Franke, S. Gonzalez, C. Lowry, M. Gadomska, J. Harman, B. Meszaros, C. Morlock, F. Romanelli, R. Wenninger, Overview of EU DEMO design and R&D activities. *Fusion Eng. Des.* **89**, 882–889 (2014).
19. C. Gormezano, A. C. C. Sips, T. C. Luce, S. Ide, A. Becoulet, X. Litaudon, A. Isayama, J. Hobirk, M. R. Wade, T. Oikawa, R. Prater, A. Zvonkov, B. Lloyd, T. Suzuki, E. Barbato, P. Bonoli, C. K. Phillips, V. Vdovin, E. Joffrin, T. Casper, J. Ferron, D. Mazon, D. Moreau, R. Bundy, C. Kessel, A. Fukuyama, N. Hayashi, F. Imbeaux, M. Murakami, A. R. Polevoi, H. E. S. John, Chapter 6: Steady state operation. *Nucl. Fusion* **47**, S285–S336 (2007).
20. D. van Houtte, G. Martin, A. Becoulet, J. Bucalossi, G. Giruzzi, G. T. Hoang, T. Loarer, B. Saoutic; Tore Supra Team, Recent fully non-inductive operation results in Tore Supra with 6 min, 1 GJ plasma discharges. *Nucl. Fusion* **44**, L11 (2004).
21. B. Wan, Recent experiments in the EAST and HT-7 superconducting tokamaks. *Nucl. Fusion* **49**, 104011 (2009).
22. Y. T. Song, J. G. Li, Y. X. Wan, B. N. Wan, P. Fu, X. Gao, B. J. Xiao, Y. P. Zhao, C. D. Hu, G. Gao, L. Q. Hu, X. Z. Gong, L. W. Xu, Y. Y. Huang, Y. W. Sun, F. K. Liu, X. J. Wang, J. S. Hu, Q. S. Hu, J. Shan, Q. X. Yang, J. X. Zheng, Z. X. Chen, X. Ji, S. K. Wang, The accomplishments and next-step plan of EAST in support of fusion. *IEEE Trans. Plasma Sci.* **42**, 415–420 (2014).
23. A. Ekedahl, L. Delpech, M. Goniche, D. Guilhem, J. Hillairet, M. Preynas, P. K. Sharmaa, J. Achard, Y. S. Bae, X. Bai, C. Balorin, Y. Baranov, V. Basiuk, A. Bécoulet, J. Belo, G. Berger-By, S. Brémond, C. Castaldo, S. Ceccuzzi, R. Cesario, E. Corbel, X. Courtois, J. Decker, E. Delmasb, X. Ding, D. Douai, C. Goletto, J. P. Gunn, P. Hertout, G. T. Hoang, F. Imbeaux, K. K. Kirov, X. Litaudon, R. Magne, J. Mailloux, D. Mazon, F. Mirizzi, P. Mollard, P. Moreau, T. Oosako,

V. Petrzilka, Y. Peysson, S. Poli, M. Prou, F. Saint-Laurent, F. Samaille, B. Saoutic, Validation of the ITER-relevant passive-active-multijunction LHCD launcher on long pulses in Tore Supra. *Nucl. Fusion* **50**, 112002 (2010).

24. J. Bucalossi, J. Achard, O. Agullo, T. Alarcon, L. Allegretti, H. Ancher, G. Antar, S. Antusch, V. Anzallo, C. Arnas, D. Arranger, J. F. Artaud, M. H. Aumeunier, S. G. Baek, X. Bai, J. Balbin, C. Balorin, T. Barbui, A. Barbuti, J. Barlerin, V. Basiuk, T. Batal, O. Baulaigue, A. Bec, M. Bécoulet, E. Benoit, E. Benard, J. M. Benard, N. Bertelli, E. Bertrand, P. Beyer, J. Bielecki, P. Bienvenu, R. Bisson, V. Bobkov, G. Bodner, C. Bottereau, C. Bouchand, F. Bouquey, C. Bourdelle, J. Bourg, S. Brezinsek, F. Brochard, C. Brun, V. Bruno, H. Bufferand, A. Bureau, S. Burles, Y. Camenen, B. Cantone, E. Caprin, S. Carpentier, G. Caulier, N. Chanet, O. Chellai, Y. Chen, M. Chernyshova, P. Chmielewski, W. Choe, A. Chomiczewska, G. Ciraolo, F. Clairet, J. Coenen, L. Colas, G. Colledani, J. Colnel, P. Coquillat, E. Corbel, Y. Corre, S. Costea, X. Courtois, T. Czarski, R. Daniel, J. Daumas, M. De Combarieu, G. De Temmerman, P. De Vries, C. Dechelle, F. Deguara, R. Dejarnac, J. M. Delaplanche, L. F. Delgado-Aparicio, E. Delmas, L. Delpech, C. Desgranges, P. Devynck, S. Di Genova, R. Diab, A. Diallo, M. Diez, G. Dif-Pradalier, M. Dimitrova, B. Ding, T. Dittmar, L. Doceul, M. Domenes, D. Douai, H. Dougnac, X. Duan, L. Dubus, N. Dumas, R. Dumont, F. Durand, A. Durif, A. Durocher, F. Durodié, A. Ekedahl, D. Elbeze, S. Ertmer, A. Escarguel, F. Escourbiac, K. Ezato, F. Faisse, N. Faure, N. Fedorczak, P. Fejoz, C. Fenzi-Bonizec, F. Ferlay, M. Firdaouss, L. Fleury, D. Flouquet, A. Gallo, Y. Gao, X. Garbet, J. Garcia, J. L. Gardarein, L. Gargiulo, P. Garibaldi, S. Garitta, J. Gaspar, E. Gauthier, P. Gavila, S. Gazzotti, F. Gely, M. Geynet, S. Gharafi, P. Ghendrih, I. Giacalone, C. Gil, S. Ginoux, S. Girard, E. Giroux, G. Giruzzi, C. Goletto, M. Goniche, T. Gray, E. Grelier, H. Greuner, E. Grigore, C. Grisolia, A. Grosjean, A. Grosman, D. Guibert, D. Guilhem, C. Guillemaut, B. Guillermin, R. Guirlet, J. P. Gunn, Y. Gunsu, T. Gyergyek, A. Hakola, J. Harris, J. C. Hatchressian, W. Helou, P. Hennequin, C. Hernandez, K. Hill, J. Hillairet, T. Hirai, G. T. Hoang, M. Houry, T. Hutter, F. Imbeaux, N. Imbert, I. Ivanova-Stanik, R. Jalageas, A. Jardin, L. Jaubert, G. Jiolat, A. Jonas, P. Joubert, A. Kirschner, C. Klepper, M. Komm, M. Koubiti, J. Kovacic, M. Kozeiha, K. Krieger, K. Krol, B. Lacroix, L. Laguardia, V. Lamaison, H. Laqua, C. Lau, Y. Lausenaz, R. Lé, M. Le Bohec, N. Lefevre, N. Lemoine, E. Lerche, M. Lewerentz, Y. Li, M. Li, A. Liang, P. Linczuk, C. Linsmeier, M. Lipa, X. Litaudon, X. Liu, J. Llorens, T. Loarer, A. Loarte, T. Loewenhoff, G. Lombard, J. Lore, P. Lorenzetto, P. Lotte, M. Lozano, B. Lu, R. Lunsford, G. Luo, P. Magaud, P. Maget, J. F. Mahieu, P. Maini, P. Malard, K. Malinowski, P. Manas, L. Manenc, Y. Marandet, J. L. Marechal, S. Marek, C. Martin, E. Martin, A. Martinez, P. Martino, D. Mazon, P. Messina, L. Meunier, D. Midou, Y. Mineo, M. Missilian, R. Mitteau, B. Mitu, P. Mollard, V. Moncada, T. Mondiere, J. Morales, M. Moreau, P. Moreau, Y. Moudden, G. Moureau, D. Mouyon, M. Muraglia, A. Nagy, T. Nakano, E. Nardon, A. Neff, F. Nespoli, J. Nichols, S. Nicollet, R. Nouailletas, M. Ono, V. Ostuni, C. Parish, H. Park, H. Parrat, J. Y. Pascal, B. Pégourié, F. P. Pellissier, Y. Peneliau, M. Peret, Y. Peysson, E. Pignoly, G. Pintsuk, R. Pitts, C. Pocheau, C. Portafaix, M. Poulos, P. Prochet, A. Puig Sitjes, M. Rasinski, G. Raup, X. Regal-Mezin, C. Reux, B. Riccardi, J. Rice, M. Richou, F. Rigollet, H. Roche, J. Romazanov, C. Ruset, R. Sabot, A. Saille, R. Sakamoto, T. Salmon, F. Samaille, A. Santagiustina, B. Santraine, Y. Sarazin, E. Serre, H. Shin, S. Shiraiwai, J. Signoret, J. Signoret, A. Simonin, O. Skalli Fettachi, Y. Song, A. Spring, P. Spuig, S. Sridhar, B. Stratton, C. Talatizi, P. Tamain, R. Tatali, M. Téna, A. Torre, L. Toulouse, J. M. Travère, W. Treutterer, E. Tsitrone, E. Unterberg, G. Urbanczyk, D. Van Eester, G. Van Rooij, S. Vartanian, J. M. Verger, L. Vermare, D. Vézinet, N. Vignal, B. Vincent, S. Vives, D. Volpe, G. Wallace, E. Wang, L. Wang, Y. Wang, Y. Wang, T. Wauters, B. Wirth, M. Wirtz, A. Wojenski, J. Wright, M. Xu, Q. Yang, H. Yang, B. Zago, Zagorski, B. Zhang, X. Zhang, X. L. Zou, Operating a full tungsten actively cooled Tokamak: Overview of WEST first phase of operation. *Nucl. Fusion* **62**, 042007 (2022).
25. F. Wagner, G. Becker, K. Behringer, D. Campbell, A. Eberhagen, W. Engelhardt, G. Fussmann, O. Gehre, J. Gernhardt, G. v. Gierke, G. Haas, M. Huang, F. Karger, M. Keilhacker, O. Klüber, M. Kornherr, K. Lackner, G. Lisitano, G. G. Lister, H. M. Mayer, D. Meisel, E. R. Müller, H. Murmann, H. Niedermeyer, W. Poschenrieder, H. Rapp, H. Röhr, F. Schneider, G. Siller, E. Speth, A. Stäbler, K. H. Steuer, G. Venus, O. Vollmer, Z. Yü, Regime of improved confinement and high beta in neutral-beam-heated divertor discharges of the ASDEX Tokamak. *Phys. Rev. Lett.* **49**, 1408–1412 (1982).
26. A. Loarte, G. Saibene, R. Sartori, M. Becoulet, L. Horton, T. Eich, A. Herrmann, M. Laux, G. Matthews, S. Jachmich, N. Asakura, A. Chankin, A. Leonard, G. Porter, G. Federici, M. Shimada, M. Sugihara, G. Janeschitz, ELM energy and particle losses and their extrapolation to burning plasma experiments. *J. Nucl. Mater.* **313–316**, 962–966 (2003).
27. M. Greenwald, R. L. Boivin, F. Bombarda, P. T. Bonoli, C. L. Fiore, D. Garnier, J. A. Goetz, S. N. Golovato, M. A. Graf, R. S. Granetz, S. Horne, A. Hubbard, I. H. Hutchinson, J. H. Irby, B. LaBombard, B. Lipschultz, E. S. Marmar, M. J. May, G. M. McCracken, P. O'Shea, J. E. Rice, J. Schachter, J. A. Snipes, P. C. Stek, Y. Takase, J. L. Terry, Y. Wang, R. Watterson, B. Welch, S. M. Wolfe, H mode confinement in Alcator C-Mod. *Nucl. Fusion* **37**, 793–807 (1997).
28. F. Ryter, W. Suttrop, B. Brusehaber, M. Kaufmann, V. Mertens, H. Murmann, A. G. Peeters, J. Stober, J. Schweinzer, H. Zohm; ASDEX Upgrade Team, H-mode power threshold and transition in ASDEX Upgrade. *Plasma Phys. Control. Fusion* **40**, 725–729 (1998).
29. D. G. Whyte, A. E. Hubbard, J. W. Hughes, B. Lipschultz, J. E. Rice, E. S. Marmar, M. Greenwald, I. Cziegler, A. Dominguez, T. Golfinopoulos, N. Howard, L. Lin, R. M. McDermott, M. Porkolab, M. L. Reinke, J. Terry, N. Tsujii, S. Wolfe, S. Wukitch, Y. Lin, I-mode: An H-mode energy confinement regime with L-mode particle transport in Alcator C-Mod. *Nucl. Fusion* **50**, 105005 (2010).
30. A. D. Liu, X. L. Zou, M. K. Han, T. B. Wang, C. Zhou, M. Y. Wang, Y. M. Duan, G. Verdoolaege, J. Q. Dong, Z. X. Wang, F. Xi, J. L. Xie, G. Zhuang, W. X. Ding, S. B. Zhang, Y. Liu, H. Q. Liu, L. Wang, Y. Y. Li, Y. M. Wang, B. Lv, G. H. Hu, Q. Zhang, S. X. Wang, H. L. Zhao, C. M. Qu, Z. X. Liu, Z. Y. Liu, J. Zhang, J. X. Ji, X. M. Zhong, T. Lan, H. Li, W. Z. Mao, W. D. Liu, Experimental identification of edge temperature ring oscillation and alternating turbulence transitions near the pedestal top for sustaining stationary I-mode. *Nucl. Fusion* **60**, 126016 (2020).
31. ITER Physics Expert Group on Confinement and Transport; ITER Physics Expert Group on Confinement Modelling and Database and ITER Physics Basis Editors, Chapter 2: Plasma confinement and transport. *Nucl. Fusion* **39**, 2175–2249 (1999).
32. E. Li, X. L. Zou, L. Q. Xu, Y. Q. Chu, X. Feng, H. Lian, H. Q. Liu, A. D. Liu, M. K. Han, J. Q. Dong, H. H. Wang, J. W. Liu, Q. Zang, S. X. Wang, T. F. Zhou, Y. H. Huang, L. Q. Hu, C. Zhou, H. X. Qu, Y. Chen, S. Y. Lin, B. Zhang, J. P. Qian, J. S. Hu, G. S. Xu, J. L. Chen, K. Lu, F. K. Liu, Y. T. Song, J. G. Li, X. Z. Gong; EAST Team, Experimental evidence of intrinsic current generation by turbulence in stationary Tokamak plasmas. *Phys. Rev. Lett.* **128**, 085003 (2022).
33. F. Ding, G.-N. Luo, X. Chen, H. Xie, R. Ding, C. Sang, H. Mao, Z. Hu, J. Wu, Z. Sun, L. Wang, Y. Sun, J. Hu; the EAST Team, Plasma–tungsten interactions in experimental advanced superconducting tokamak (EAST). *Tungsten* **1**, 122–131 (2019).
34. A. Gibson; the JET Team, Deuterium–tritium plasmas in the Joint European Torus (JET): Behavior and implications. *Phys. Plasmas* **5**, 1839 (1998).
35. S. Ishida; JT-60 Team, JT-60U high performance regimes. *Nucl. Fusion* **39**, 1211 (1999).
36. K. M. Mcguire, C. W. Barnes, S. Batha, M. Beer, M. G. Bell, R. E. Bell, A. Belov, H. Berk, S. Bernabei, M. Bitter, B. Breizman, N. L. Bretz, R. Budny, C. E. Bush, J. Callen, S. Cauffman, C. S. Chang, Z. Chang, C. Z. Cheng, G. A. Cottrell, D. S. Darrow, R. O. Dendy, W. Dorland, H. Duong, P. C. Efthimion, D. Ernts, H. Evenson, N. J. Fisch, R. Fisher, R. J. Fonck, C. Forest, E. D. Fredrickson, G. Y. Fu, H. P. Furth, N. N. Gorelenkov, V. Ya. Goloborod'Ko, B. Grek, L. R. Grisham, G. W. Hammett, G.R. Hanson, R. J. Hawryluk, W. Heidbrink, H.W. Herrmann, M. Herrmann, K. W. Hill, J. Hogan, B. Hooper, J. C. Hosea, W.A. Houlberg, M. Hughes, R. A. Hulse, D. L. Jassby, F. C. Jobes, D. W. Johnson, R. Kaita, S. Kaye, J. Kesner, J. S. Kim, M. Kissick, A. V. Krasilnikov, H. Kumar, N. T. Lam, P. Lamarche, B. LeBlanc, F. M. Levinton, C. Ludescher, J. Machuzak, R. J. Majeski, J. Manickam, D. K. Mansfield, M. Mauel, E. Mazzucato, J. McChesney, D. C. McCune, G. McKee, D. M. Meade, S. S. Medley, R. Mika, D. R. Mikkelsen, S. V. Mirnov, D. Mueller, Y. Nagayama, G. A. Navratil, R. Nazikian, M. Okabayashi, D. K. Owens, H. K. Park, W. Park, P. Parks, S.F. Paul, M. P. Petrov, C.K. Phillips, M. Phillips, P. Phillips, A. T. Ramsey, M. H. Redi, G. Rewoldt, S. Reznik, A. L. Roquemore, J. Rogers, E. Ruskov, S. A. Sabbagh, M. Sasao, G. Schilling, J. Schivell, G. L. Schmidt, S. D. Scott, I. Semenov, T. Senko, S. Sesnic, C. H. Skinner, T. Stevenson, E. J. Strait, B.C. Stratton, J. D. Strachan, W. Stodiek, E. Synakowski, H. Takahashi, W. Tang, G. Taylor, J. Terry, M. E. Thompson, S. Von Goeler, A. Von Halle, R. T. Walters, S. Wang, R. White, R. M. Wieland, M. Williams, J. R. Wilson, K. L. Wong, G. A. Wurden, M. Yamada, V. Yavorski, K. M. Young, L. Zakharov, M. C. Zarnstorff, S. J. Zweben, Physics of high performance deuterium-tritium plasmas in TFTR, in *Fusion Energy 1996 (Proc. 16th Int. Conf. Montreal, 1996)* (IAEA, 1997), vol. 1.
37. M. Kikuchi, M. Azumi, *Frontiers in Fusion Research II: Introduction to Modern Tokamak Physics* (Springer International Publishing, 2015).
38. J. D. Lawson, Some criteria for a power producing thermonuclear reactor. *Proc. Phys. Soc. B.* **70**, 6–10 (1957).
39. EUROfusion, https://www.euro-fusion.org/.
40. H. Y. Guo, J. Li, X. Z. Gong, B. N. Wan, J. S. Hu, L. Wang, H. Q. Wang, J. E. Menard, M. A. Jaworski, K. F. Gan, S. C. Liu, G. S. Xu, S. Y. Ding, L. Q. Hu, Y. F. Liang, J. B. Liu, G. N. Luo, H. Si, D. S. Wang, Z. W. Wu, L. Y. Xiang, B. J. Xiao, L. Zhang, X. L. Zou, D. L. Hillis, A. Loarte, R. Maingi; the EAST Team, Approaches towards long-pulse divertor operations on EAST by active control of plasma–wall interactions. *Nucl. Fusion* **54**, 013002 (2013).
41. B. J. Xiao, D. A. Humphreys, M. L. Walker, A. Hyatt, J. A. Leuer, D. Mueller, B. G. Penaflor, D. A. Pigrowski, R. D. Johnson, A. Welander, Q. P. Yuan, H. Z. Wang, J. R. Luo, Z. P. Luo, C. Y. Liu, L. Z. Liu, K. Zhang, EAST plasma control system. *Fusion Eng. Des.* **83**, 181–187 (2008).
42. Q. P. Yuan, J. Y. Tang, B. Penaflor, R. Johnson, K. Wu, D. Piglowski, R. R. Zhang, B. J. Xiao, W. T. Chai, I. Anyanetu, B. Sammuli, M. Kostuk, Upgrade of EAST plasma control system for steady-state advanced operation. *Fusion Eng. Des.* **129**, 109–114 (2018).
43. Q. Zang, J. Zhao, L. Yang, Q. Hu, X. Xi, X. Dai, J. Yang, X. Han, M. Li, C. L. Hsieh, Upgraded multipulse laser and multipoint Thomson scattering diagnostics on EAST. *Rev. Sci. Instrum.* **82**, 063502 (2011).
44. H. Q. Liu, J. P. Qian, Y. X. Jie, W. X. Ding, D. L. Brower, Z. Y. Zou, W. M. Li, H. Lian, S. X. Wang, Y. Yang, L. Zeng, T. Lan, Y. Yao, L. Q. Hu, X. D. Zhang, B. N. Wan, Initial measurements of plasma current and electron density profiles using a polarimeter/interferometer (POINT) for long pulse operation in EAST (invited). *Rev. Sci. Instrum.* **87**, 11D903 (2016).

45. J. P. Qian, L. L. Lao, H. Q. Liu, W. X. Ding, L. Zeng, Z. P. Luo, Q. L. Ren, Y. Huang, J. Huang, D. L. Brower, K. Hanada, D. L. Chen, Y. W. Sun, B. Shen, X. Z. Gong, B. J. Xiao, B. N. Wan, EAST equilibrium current profile reconstruction using polarimeter-interferometer internal measurement constraints. *Nucl. Fusion* **57**, 036008 (2017).
46. L. Zhang, S. Morita, Z. Wu, Z. Xu, X. Yang, Y. Cheng, Q. Zang, H. Liu, Y. Liu, H. Zhang, T. Ohishi, Y. Chen, L. Xu, C. Wu, Y. Duan, W. Gao, J. Huang, X. Gong, L. Hu, A space-resolved extreme ultraviolet spectrometer for radial profile measurement of tungsten ions in the Experimental Advanced Superconducting Tokamak. *Nucl. Instrum. Methods Phys. Res. A* **916**, 169–178 (2019).
47. K. Chen, L. Xu, L. Hu, Y. Duan, X. Li, Y. Yuan, S. Mao, X. Sheng, J. Zhao, 2-D soft x-ray arrays in the EAST. *Rev. Sci. Instrum.* **87**, 063504 (2016).
48. C. Zhou, A. D. Liu, X. H. Zhang, J. Q. Hu, M. Y. Wang, H. Li, T. Lan, J. L. Xie, X. Sun, W. X. Ding, W. D. Liu, C. X. Yu, Microwave Doppler reflectometer system in the experimental advanced superconducting tokamak. *Rev. Sci. Instrum.* **84**, 103511 (2013).
49. X. M. Zhong, X. L. Zou, A. D. Liu, Y. T. Song, G. Zhuang, E. Z. Li, B. Zhang, J. Zhang, C. Zhou, X. Feng, Y. M. Duan, R. Ding, H. Q. Liu, B. Lv, L. Wang, L. Q. Xu, L. Zhang, H. L. Zhao, Q. Zang, T. Zhang, B. J. Ding, M. H. Li, C. M. Qin, X. J. Wang, X. J. Zhang; EAST Team, Characterization of pedestal burst instabilities during I-mode to H-mode transition in the EAST Tokamak. *Nucl. Fusion* **62**, 066046 (2022).
50. J. C. Xu, L. Wang, G. S. Xu, G. N. Luo, D. M. Yao, Q. Li, L. Cao, L. Chen, W. Zhang, S. C. Liu, H. Q. Wang, M. N. Jia, W. Feng, G. Z. Deng, L. Q. Hu, B. N. Wan, J. Li, Y. W. Sun, H. Y. Guo, Upgrade of Langmuir probe diagnostic in ITER-like tungsten mono-block divertor on experimental advanced superconducting tokamak. *Rev. Sci. Instrum.* **87**, 083504 (2016).
51. F. Wang, G. Li, S. Li, Y. Zhu, Y. Wang, A continuous data acquisition system based on CompactPCI for EAST Tokamak. *IEEE Trans. Nucl. Sci.* **57**, 669–672 (2010).
52. G. Z. Zuo, J. S. Hu, J. G. Li, N. C. Luo, L. E. Zakharov, L. Zhang, A. Ti, First results of lithium experiments on EAST and HT-7. *J. Nucl. Mater.* **415**, S1062–S1066 (2011).
53. D. K. Mansfield, A. L. Roquemore, H. Schneider, J. Timberlake, H. Kugel, M. G. Bell, A simple apparatus for the injection of lithium aerosol into the scrape-off layer of fusion research devices. *Fusion Eng. Des.* **85**, 890–895 (2010).
54. Y. W. Yu, J. S. Hu, G. Z. Zuo, Z. Sun, L. Wang, W. Xu, J. R. Wang, B. Cao, W. Gao, J. C. Xu, J. G. Li; the EAST Team, Control of hydrogen content and fuel recycling for long pulse high performance plasma operation in EAST. *Nucl. Fusion* **59**, 126036 (2019).
55. G. S. Xu, B. N. Wan, J. Li, X. Z. Gong, J. S. Hu, J. F. Shan, H. Li, D. K. Mansfield, D. A. Humphreys, V. Naulin, Study on H-mode access at low density with lower hybrid current drive and lithium-wall coatings on the EAST superconducting tokamak. *Nucl. Fusion* **51**, 072001 (2011).
56. T. Petrie, M. Fenstermacher, C. Holcomb, T. Osborne, S. Allen, J. Ferron, H. Guo, C. Lasnier, A. Leonard, T. Luce, M. A. Makowski, A. G. McLean, D. C. Pace, W. M. Solomon, F. Turco, M. A. Van Zeeland, J. G. Watkins, Results from core-edge experiments in high power, high performance plasmas on DIII-D. *Nucl. Mater. Energy* **12**, 1141–1145 (2017).
57. J. Li, Y. Wan; the EAST Team, The experimental advanced superconducting tokamak. *Engineering* **7**, 1523–1528 (2021).
58. J. Wei, W. G. Chen, W. Y. Wu, Y. N. Pan, D. M. Gao, S. T. Wu, Y. Wu, The superconducting magnets for EAST tokamak. *IEEE Trans. Appl. Supercond.* **20**, 556–559 (2010).
59. S. T. Wu; the EAST Team, An overview of the EAST project. *Fusion Eng. Des.* **82**, 463–471 (2007).
60. P. Fu, Z. Z. Liu, G. Gao, L. Yang, Z.Q. Song, L. W. Xu, J. Tao, X. N. Liu, in *2010 5th IEEE Conference on Industrial Electronics and Applications* (IEEE, 2010), pp. 457–462.
61. F. K. Liu, J. G. Li, J. F. Shan, M. Wang, L. Liu, L. M. Zhao, H. C. Hu, J. Q. Feng, Y. Yang, H. Jia, X. J. Wang, Z. G. Wu, W. D. Ma, Y. Y. Huang, H. D. Xu, J. Zhang, M. Cheng, L. Xu, M. H. Li, Y. C. Li, Q. Zang, G. Q. Li, B. J. Ding, Development of 4.6 GHz lower hybrid current drive system for steady state and high performance plasma in EAST. *Fusion Eng. Des.* **113**, 131–138 (2016).
62. C. Hu, Y. Xie, Y. Xie, S. Liu, Y. Xu, L. Liang, C. Jiang, P. Sheng, Y. Gu, J. Li, Z. Liu, Overview of development status for EAST-NBI system. *Plasma Sci. Technol.* **17**, 817–825 (2015).
63. X. J. Zhang, H. Yang, C. M. Qin, S. Yuan, Y. P. Zhao, Y. S. Wang, L. N. Liu, Y. Z. Mao, Y. Cheng, X. Z. Gong, G. S. Xu, Y. T. Song, J. G. Li, B. N. Wan, K. Zhang, B. Zhang, L. Ai, G. X. Wang, Y. Y. Guo, First experimental results with new ICRF antenna in EAST. *Nucl. Fusion* **62**, 086038 (2022).
64. B. N. Wan, X. Z. Gong, Y. Liang, N. Xiang, G. S. Xu, Y. Sun, L. Wang, J. P. Qian, H. Q. Liu, B. Zhang, T. Y. Xia, J. Huang, R. Ding, T. Zhang, G. Z. Zuo, Z. Sun, L. Zeng, X. J. Zhang, Q. Zang, B. Lyu, A. M. Garofalo, G. Q. Li, K. D. Li, Q. Q. Yang, Advances in the long-pulse steady-state high beta H-mode scenario with active controls of divertor heat and particle fluxes in EAST. *Nucl. Fusion* **62**, 042010 (2022).
65. J. Zheng, J. Qin, K. Lu, M. Xu, X. Duan, G. Xu, J. Hu, X. Gong, Q. Zang, Z. Liu, L. Wang, R. Ding, J. Chen, P. Li, L. Xue, L. Cai, Y. Song, Recent progress in Chinese fusion research based on superconducting tokamak configuration. *Innovation (Camb.)* **3**, 100269 (2022).
66. Y. Shi, F. Wang, B. Wan, M. Bitter, S. Lee, J. Bak, K. Hill, J. Fu, Y. Li, W. Zhang, A. Ti, B. Ling, Imaging x-ray crystal spectrometer on EAST. *Plasma Phys. Control. Fusion* **52**, 085014 (2010).
67. X. Han, X. Liu, Y. Liu, C. W. Domier, N. C. Luhmann, E. Z. Li, L. Q. Hu, X. Gao, Design and characterization of a 32-channel heterodyne radiometer for electron cyclotron emission measurements on experimental advanced superconducting tokamak. *Rev. Sci. Instrum.* **85**, 073506 (2014).
68. X. Zhu, L. Zeng, H. Liu, Y. Jie, S. Zhang, J. Hu, X. Gao, Reconstruction of the density profile for the EAST tokamak based on polarimeter/interferometer and microwave reflectometer systems. *Plasma Sci. Technol.* **17**, 733–737 (2015).
69. S. Zhang, X. Gao, B. Ling, Y. Wang, T. Zhang, X. Han, Z. Liu, J. Bu, J. Li, Density profile and fluctuation measurements by microwave reflectometry on EAST. *Plasma Sci. Technol.* **16**, 311–315 (2014).
70. X. Feng, A. D. Liu, C. Zhou, M. Y. Wang, J. Zhang, Z. Y. Liu, Y. Liu, T. F. Zhou, S. B. Zhang, D. F. Kong, L. Q. Hu, J. X. Ji, H. R. Fan, H. Li, T. Lan, J. L. Xie, W. Z. Mao, Z. X. Liu, W. X. Ding, G. Zhuang, W. D. Liu, Five-channel tunable W-band Doppler backscattering system in the experimental advanced superconducting tokamak. *Rev. Sci. Instrum.* **90**, 024704 (2019).
71. H. Xu, X. Wang, J. Zhang, F. Liu, Y. Huang, J. Shan, W. Xu, M. Li, J. Lohr, Y. A. Gorelov, J. P. Anderson, Y. Zhang, D. Wu, H. Hu, Y. Yang, J. Feng, Y. Tang, B. Li, W. Ma, Z. Wu, J. Wang, L. Zhang, F. Guo, H. Sun, X. Yan; EAST Team, Recent progress of the development of a long pulse 140GHz ECRH system on EAST. *EPJ Web Conf.* **203**, 04002 (2019).
72. H. Xu, W. Xu, D. Wu, M. Li, X. Wang, L. Zhang, J. Lohr, J. Doane, J. P. Anderson, Y. A. Gorelov, J. Wang, Y. Hou, W. He, T. Zhang, ECRH system upgrade design using dual frequency gyrotrons for EAST. *Fusion Eng. Des.* **164**, 112222 (2021).
73. F. Wang, Y. Chen, S. Li, Y. Wang, X. Y. Sun, F. Yang, in *2016 IEEE-NPSS Real Time Conference (RT)* (IEEE, 2016), pp. 1–3.
74. D. Wang, Y. Ren, D. Chen, T. Tang, X. Gao, Eddy current analysis of TF coil case for EAST. *IEEE Trans. Appl. Supercond.* **30**, 1–9 (2020).
75. B. J. Xiao, Z. P. Luo, H. Li, G. Q. Li, L. Wang, Z. L. Wang, G. S. Xu, D. M. Yao, Z. B. Zhou, G. Calabrò, F. Crisanti, A. Castaldo, R. Lombroni, S. Minucci, G. Ramogida, Progress on in-vessel poloidal field coils optimization design for alternative divertor configuration studies on the EAST tokamak. *Fusion Eng. Des.* **146**, 2149–2152 (2019).
76. Z. Zhou, Q. Zhang, Z. Zhu, P. Zhu, L. Hu, in *IOP Conference Series: Materials Science and Engineering* (IOP Publishing, 2019), vol. 502, p. 012121.
77. Z. Zhou, Q. Zhang, P. Zhu, K. Wu, Z. Zhu, L. Sheng, K. Yuan, in *IOP Conference Series: Materials Science and Engineering* (IOP Publishing, 2022), 1240, p. 012070.
78. G. Z. Zuo, J. S. Hu, J. G. Li, Z. Sun, D. K. Mansfield, L. E. Zakharov, Lithium coating for H-mode and high performance plasmas on EAST in ASIPP. *J. Nucl. Mater.* **438**, S90–S95 (2013).

Acknowledgments: We thank A. Hubbard (MIT, USA) for fruitful discussions. We also thank Sino-US fusion cooperation and Sino-France fusion cooperation for strong support on comprehensive collaboration research. **Funding:** This work is supported by the National Key R&D Program of China (grant nos. 2021YFE030203 and 2019YFE03040003). This work was also partly supported by China National Funds for Distinguished Young Scientists with no. 51525703. This work is also supported by the Users with Excellence Program of Hefei Science Center CAS under grant no. 2020HSC-UE009. This work is also supported by the EAST Performance Improvement project E05AH105I1. This work is also partly supported by U.S. DOE under E05AH105I1, DE-FC02-04ER54698, DE-SC0010492, and DE-SC0010685. **Author contributions:** Conceptualization: Y.So, X.Zo., A.B., R.B., P.B., T.H., R.M., X.Zh., A.L., and E.L. Methodology: Y.So, X.Zo., X.G., J.Q., X.Zh., A.L., E.L., R.D., J. Huang, H. Liu, Y.Su., L.X., B.Z., S.W., Y.C., T.Z., Y.D., H. Lian, Xuexi Zhang, Y.J., L.Ze., B.L., X. Wang, B.D., M.L., Xinjun Zhang, C.Q., and EAST team. Investigation: Y.So, X.Zo., X.Zh., A.L., E.L., B.Z., H. Liu, L.W., L.Zh., L.X., S.W., Y.C., T.Z., Y.D., Xuexi Zhang, Y.J., L.Ze., B.L., X. Wang, B.D., M.L., Xinjun Zhang, C.Q., and EAST team. Visualization: Y.So, X.Zo., Q.Z., H. Liu, L.W., L.Zh., G.L., L.X., S.W., Y.C., T.Z., Y.D., H. Lian, Xuexi Zhang, Y.J., L.Ze., B.X., Y. Huang, Y. Wang, B.S., N.X., Y. Wu, J.W., W.X., J.Z., L.H., D.Y., Y. Hu, G.Z., Q.Y., Z.Z., M.W., H.X., Y.X., Z.W., and EAST team. Funding acquisition: Y.So. Project administration: Y.So. Supervision: Y.So, J.C., G.X., J. Hu, K.L., F.L., X. Wu, B.W., and J.L. Writing—original draft: Y.So and X.Zo. Writing—review and editing: Y.So, X.Zo., A.B., R.B., P.B., T.H., R.M., A.G., T.O., T.L., S.G.B., and G.W. **Competing interests:** The authors declare that they have no competing interests. **Data and materials availability:** All data needed to evaluate the conclusions in the paper are present in the paper and/or the Supplementary Materials.

Submitted 14 April 2022
Accepted 7 November 2022
Published 6 January 2023
10.1126/sciadv.abq5273